PHYSICAL REVIEW A VOLUME 46, NUMBER 2 15 JULY 1992

Structural and dynamical transformations between neighboring dense microemulsion phases

M. Kotlarchyk
Department of Physics, Rochester Institute of Technology, Rochester, New York 14623

E. Y. Sheu
Texaco Research Center, P.O. Box 509, Beacon, New York 12508

M. Capel
Department of Biology, Brookhaven National Laboratory, Upton, New York 11973
(Received 2 March 1992)

A small-angle x-ray scattering (SAXS) study of dense AOT-water-decane microemulsions [AOT denotes sodium bis(2-ethylhexyl) sulfosuccinate] was undertaken in order to delineate clearly the phase behavior and corresponding structural transitions for AOT-plus-water volume fractions ranging from $\phi=0.60$ to 0.95. Spectra were collected for temperatures between $T=3$ and 65 °C. The resulting T-vs-ϕ phase diagram indicates three distinct structural domains when the water-to-AOT molar ratio is fixed at $W=40.8$, namely, the previously investigated L_2 droplet phase, a high-temperature L_α lamellar phase, and a low-temperature L_3 phase consisting of randomly connected lamellar sheets. A significantly wide coexistence region accompanies the droplet-to-lamellar phase transition, which is demonstrated to be first order. For W between 15 and 40, an analysis of the lamellar structure using a one-dimensional paracrystal model produces a Hosemann g factor indicative of an approximately constant variation in the lamellar spacing of about 8%. The SAXS study was supplemented by dielectric-relaxation, shear-viscosity, and quasielastic light-scattering measurements in order to substantiate the observed phase transitions and further our understanding of the structural and dynamical properties of the L_3 phase. It was found that the L_3 phase exhibits Newtonian behavior up to a shear rate of 790 s^{-1}, in contradiction to previous theoretical considerations. The phase exhibits two distinct relaxation modes. A relaxation time of ~1 ms characterizes the Brownian motion of a single lamellar sheet, while the motion of the entire interconnected sheet assembly has a relaxation time on the order of 1 s.

PACS number(s): 64.80.Gd, 82.70.Dd, 61.10.Lx, 61.30.Eb

I. INTRODUCTION

In recent years, the AOT-water-oil system [AOT denotes sodium bis(2-ethylhexyl) sulfosuccinate] has been a workhorse for the study of microemulsions [1]. Experimental investigations into the properties of this system have led to significant advances in understanding phase transitions, critical phenomena, percolation theory, and the role of interparticle interactions on the structure and dynamics of colloidal and molecular fluids [2,3]. This system presents a particularly useful model because the AOT surfactant provides a high degree of solubilization of oil and water without the addition of other surface active components (or cosurfactants), thus leading to the formation of thermodynamically stable single-phase dispersions over a wide range of compositions and temperatures. The detailed phase diagram for various values of the water-to-AOT molar ratio (W) has been constructed for AOT-plus-water volume fractions (ϕ) less than ~0.6. At $W=40.8$, scattering studies [4–6] near room temperature have conclusively demonstrated that a polydisperse (~22%) L_2 water-in-oil droplet phase persists at all volume fractions. Here, the droplets assume a mean radius of about 50 Å, but the precise size and polydispersity depends on the molar ratio W. For volume fractions below about 0.4, a phase separation into two coexisting droplet microemulsion phases occurs when the temperature of the single-phase system is raised above a certain temperature [7]. The two resulting phases contain identical droplet structures, but different droplet number densities. By viewing the droplets as playing the same role as the individual molecules in a single-component simple fluid, one can view the phase-separation process as analogous to that of a liquid-gas-type phase transition. Unlike the latter system, however, the microemulsion coexistence curve exhibits a lower consolute temperature. This is due to the increase in attractive interactions between droplets as the temperature is raised.

For volume fractions greater than about 0.6, however, only limited phase information has been reported. For example, at room temperature with $W=40.8$, it is known that after passing through a glass transition point near a volume fraction of 0.65, the L_2 phase extends out to a volume fraction of 0.75 [5,8]. At higher concentrations and temperatures it is generally believed that the system makes a liquid-solid-type transition into a smectic swollen lamallar L_α phase [5,9]. However, detailed phase and structural data is absent from the literature.

In this study, we have collected a comprehensive set of small-angle x-ray scattering (SAXS) spectra from the

AOT-water-decane system with the aim of mapping out the phase transitions and corresponding structural transformations associated with the dense microemulsion phases. The study covered the range $0.60 \leq \phi \leq 0.95$ for temperatures between 3 and 65 °C. The value of W was maintained at 40.8 for most of the measurements, but supplementary data at other W values were also collected. Figure 1 (to be more fully discussed in Sec. III) illustrates the previously unrealized rich phase structure of this system at high concentrations, as determined by the SAXS measurements at $W=40.8$.

A portion of this paper describes our analysis of the lamellar L_α phase from the x-ray intensity spectra. Structural information is extracted both from a direct analysis of the positions and heights of the observed scattering peaks and by fitting the SAXS spectra to a one-dimensional paracrystal model of randomly oriented microdomains containing flat lamellar sheets.

Of special interest is the isotropic phase labeled L_3, which is newly observed in the dense region of this system. It is characterized by noticeable streaming birefringence upon gentle shaking, and has become known as the "anomalous isotropic phase" [10–12]. Like the L_3 phase studied in other systems, the one presently observed occurs in the vicinity of a lamellar phase. However, unlike the situation in nonionic surfactant systems [13] where the L_3 phase forms at temperatures above that of the L_α phase, the phase we encounter forms at temperatures below. Although scattering studies show that generally the L_3 phase possesses a locally flat bilayer structure similar to that of the L_α phase, there is evidence for the existence of a high density of interconnecting passages between adjacent lamellar sheets [11,12,14]. The resulting topology is a bicontinuous one. However, a simple model of the L_3 phase predicts that the rheology of the phase should be largely governed by the time scale for the breakage and restoration of the interconnecting passages under shear [15–18]. Surprisingly, however, a recent experimental study [19] of the L_3-phase shear viscosity shows that its behavior remains perfectly Newtonian up to a shear rate of 200 s^{-1}, contrary to the theoretical expectation of a shear-induced isotropic-to-lamellar phase transition [16]. Conductivity measurements on the L_3 phase also exist [10,13,20], but generally provide only qualitative information about the structure.

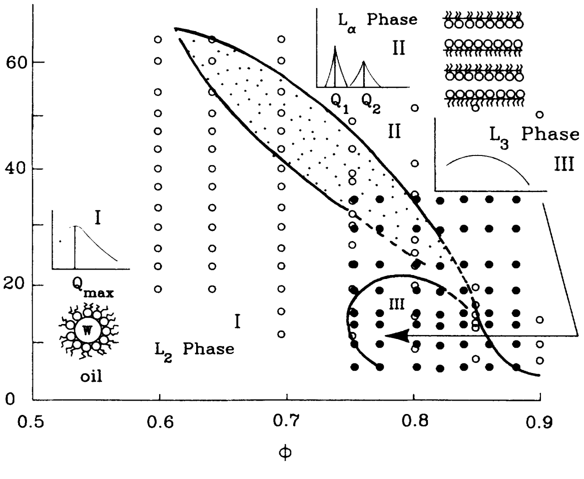

FIG. 1. Phase diagram of dense AOT-water-decane system for a water-to-AOT molar ratio of $W=40.8$. The ordinate is the temperature and the abscissa is the AOT-plus-water volume fraction. SAXS measurements were performed at points marked by circles: Oak Ridge National Laboratory measurements (○), National Synchroton Light Source measurements (●). Regions corresponding to the droplet (L_2), lamellar (L_α), and randomly connected lamellar (L_3) phases are indicated, along with their basic SAXS spectral features. The dotted area is the L_2/L_α coexistence region. The phases within the dashed boundaries are not yet identified.

Our present investigation includes systematic measurements of the dielectric-relaxation, shear-viscosity, and quasielectric light-scattering characteristics of the observed L_3 phase. In addition to corroborating some of the x-ray determined phase transitions, analysis of the data elucidates a number of central features related to the structural and dynamical properties of the L_3 phase.

II. EXPERIMENTS

A. Samples

The AOT used in the experiments was obtained from Fluka Chemical Co. with >99% purity. The decane oil was of high-pressure liquid chromatography grade and the water was distilled and deionized (resistivity >18 $M\Omega/cm^2$).

SAXS intensity spectra from samples containing purified surfactant (following the procedure described in Ref. [5]) were essentially indistinguishable from spectra collected using samples prepared without surfactant purification. We therefore used the unpurified form of AOT to prepare all of the samples in this study, except those investigated by the quasielastic light-scattering technique.

The composition of each sample was specified by the water-to-AOT molar ratio (W) and the AOT-plus-water volume fraction (ϕ). When calculating these quantities, the AOT molecular weight and volume were taken to be 444.5 g/mole and 612 Å^3/molecule, respectively.

B. Experimental techniques

1. *Small-angle x-ray scattering*

SAXS spectra were collected on the 10-m small-angle scattering spectrometer at the Oak Ridge National Laboratory (ORNL) and on the X12B beam line of the National Synchrotron Light Source (NSLS) at the Brookhaven National Laboratory. For the ORNL experiments, the x-ray generator used a Rigaku-Denki rotating anode with a copper target operating at 4.8 kW. A pyrolytic graphite moderator was used to select the K_α wavelength of 1.54 Å. A series of pinhole collimators produced a 1-mm^2 beam spot at the sample position and the sample-to-detector distance was fixed at 216 cm. The incident beam flux was of order 10^7 photons/s at the sample position. A 20×20 cm^2 two-dimensional position-sensitive proportional counter with 64×64 pixels was used for x-ray detection. The beam stop was 1 cm in diameter. With this configuration, the instrument covers a range of scattering vectors (**Q**) with magnitudes between 0.01 and 0.25 Å^{-1}, and a resolution ΔQ of about 0.005 Å^{-1}. [In a small-angle scattering experiment, Q is equal to $(4\pi/\lambda)\sin(\theta/2)$, where λ is the wavelength of incident x rays and θ is the scattering angle.] The ORNL measurements were performed for a range of microemulsion volume fractions between $\phi=0.60$ and 0.95, at a range of temperatures between $T=3$ and 65°C.

A parallel series of SAXS measurements performed on the NSLS small-angle scattering spectrometer were used to fill in more completely the picture of the phase diagram in the region corresponding to $0.75 \leq \phi \leq 0.95$ and $3 \leq T \leq 35\,°\text{C}$ (see Fig. 1). At the X12B beam line, a photon wavelength of 1.38 Å was selected from the synchrotron radiation by using a double crystal Si(111) monochromator. Collimation was provided by a defining-slit block and an x,y guard-slit array positioned 4 m downstream. The resulting beam was doubly focused to a spot size of 0.5×0.5 mm^2 full width at half maximum. The flux incident on the sample was of order 10^{11} photons/s. The scattered x rays were detected using a 10-cm linear delay-line position-sensitive detector (vertical acceptance of 2 cm) and a sample-to-detector distance of 93 cm. Data were collected on a pulse-height analyzer capable of handling an acquisition rate of 5×10^5 events/s. The spectrometer configuration covered a Q range of 0.008–0.25 Å^{-1}.

For both sets of experiments, samples were contained in 1-mm-path-length vacuum-tight aluminum cells with two 0.0005-in.-thick Kapton sheets as windows. During SAXS measurements, temperature was controlled to within ±0.1 °C with a water-bath-temperature controller. Each spectrum was corrected for transmission, dark current, empty-cell scattering, and spatial nonuniformity of detector sensitivity. The ORNL data arrays were radially averaged, and a calibrated polyethylene standard of known cross section at the scattering peak position was used for absolute intensity calibration.

2. *Dielectric-relaxation measurements*

The dielectric-relaxation measurements were performed using an HP4192A low-frequency impedance analyzer with frequency ranging from 5 to 13 MHz, in conjunction with an immersion-type cell from Rosemount Analytical. The cell consists of four electrodes coated with platinum black for the prevention of electron polarization near the plate surfaces. A Haake F3 water-bath-temperature controller with ±0.1 °C accuracy was used.

3. *Viscosity measurements*

The viscosity was measured as a function of shear rate using a Rheometrics Fluids Spectrometer with a torque range of 0.002–100 g cm, in conjunction with a Couette cell. By proper adjustment and calibration of the bob length, the viscosity was measured at shear rates up to about 1500 s^{-1}. A programmable water-bath-temperature controller with ±0.05 °C accuracy was used. Samples were allowed to stabilize for 30 min after each temperature ramping to insure system equilibration. A cover was used for the Couette cell to prevent sample evaporation.

4. *Quasielastic light scattering*

In order to characterize the dynamic relaxation within the L_3 phase, dynamic light-scattering measurements were performed. A vertically polarized 15 mW He-Ne laser ($\lambda=6328$ Å) was used with a Brookhaven Instruments model BI-200SM goniometer system and a model BI-2030AT digital correlator having 128 channels. The scattering angle was fixed at 90°. By varying the sampling time per channel, both fast and slow relaxation modes could be detected. Samples were contained in round quartz cells and immersed in toluene index-matching fluid. A water-bath-temperature controller with ±0.1 °C accuracy was used.

III. BASIC FEATURES AND INTERPRETATION OF SAXS SPECTRA

SAXS intensity spectra obtained at ORNL are displayed in Fig. 2 for microemulsions with $W=40.8$. An examination of the evolution of the spectra as the temperature is varied at each volume fraction indicates the existence of three distinct phases, each with its own characteristic scattering features, as typified by the inset sketches drawn in the Fig. 1 phase diagram. First, there is an L_2 droplet phase characterized by a spectrum with a single pronounced peak at position $Q_{\max}$. This phase is composed of polydisperse water-in-oil droplets (mean diameter ~100 Å) coated with AOT surfactant [5]. A second phase exhibits two scattering peaks, i.e., a first- and second-order peak, at Q_1 and Q_2, respectively, with $Q_2=2Q_1$. This signals the lamellar structure of the L_α phase. The third phase produces a broad diffused peak covering the entire Q range of the experiment. It is difficult to characterize the structure of this phase based on the SAXS spectra alone, but the results of the relaxation studies described in Sec. V seem to confirm the hypothesis that this is the so-called L_3 phase, containing randomly connected lameller sheets.

The characteristic features of SAXS spectra from both the ORNL and NSLS experiments were used to map out the Fig. 1 phase diagram. The phases within the dashed boundaries are not yet identified. At $\phi=0.60$, a pure L_2 droplet structure persists over the entire measured temperature range. For higher volume fractions, a coexistence region appears between the L_2 and L_α phases. This region is absent from the previously reported phase diagram [5]. Its existence is illustrated, for example, by sequentially following the changes in the $\phi=0.76$ intensity spectra as the temperature is increased. The microemulsion exhibits a droplet structure up to about 35 °C, at which point the lamellar structure begins to develop and coexist with the droplet phase, as evidenced by the competition between the droplet peak and the two emerging lamellar peaks. This coexistence region extends up to near 50°C, above which only the lamellar structure is observed. A similar structural evolution is observed for $\phi=0.80$, except the coexistence region at this volume fraction spans a narrower temperature range, i.e., about 27.5 to 35 °C. Figure 3 shows both the position of the droplet peak ($Q_{\max}$) and the corresponding peak intensity [$I(Q_{\max})$] as a function of temperature for $\phi=0.76$. The discontinuity in both these quantities at about 36 °C clearly illustrates that the transition between the droplet

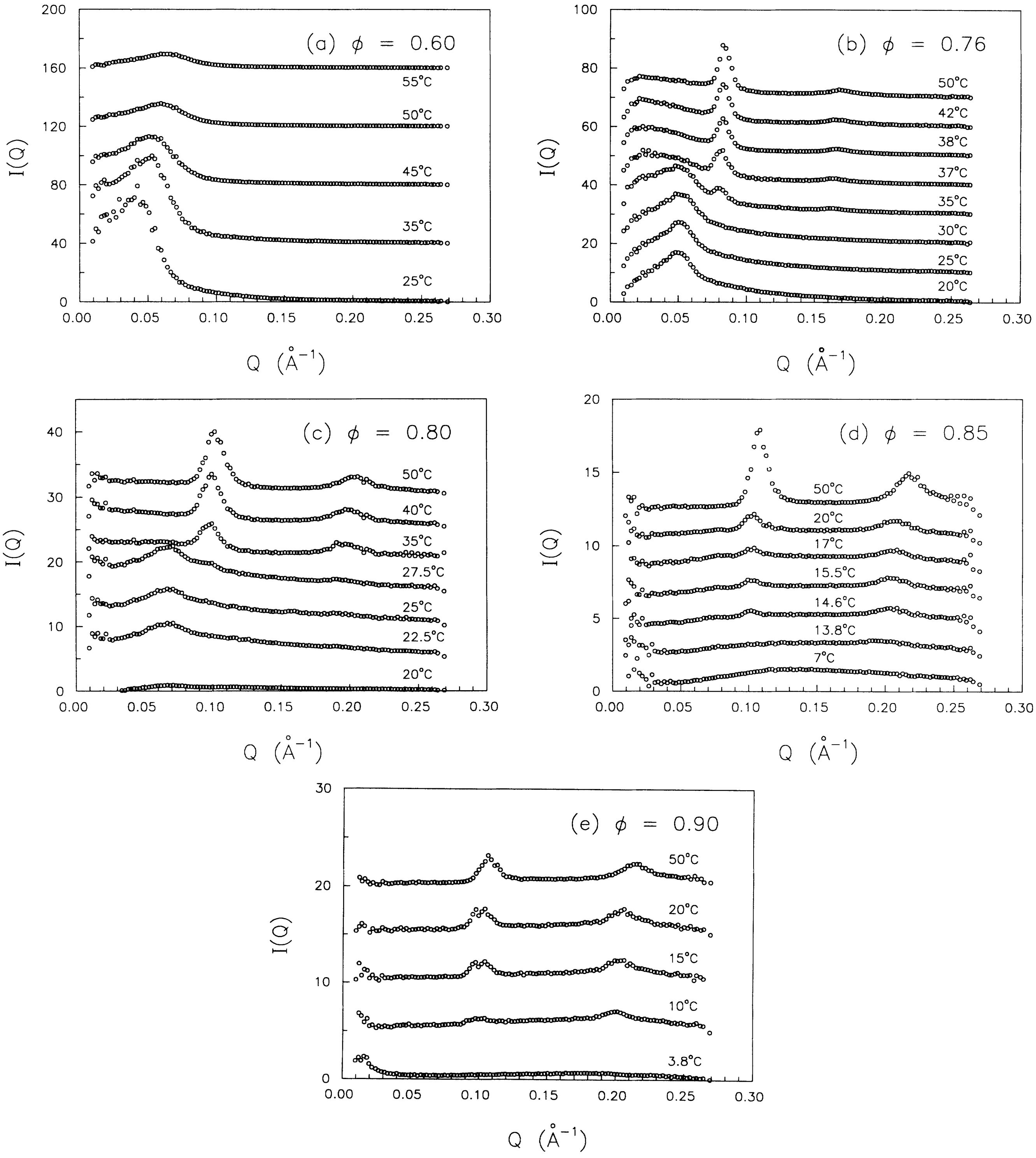

FIG. 2. Temperature evolution of the $W=40.8$ SAXS intensity spectra collected at the ORNL 10-m spectrometer for various volume fractions in the range 0.60–0.90. (The various spectra are offset vertically for display purposes.)

and lamellar phases is a first-order one. For $\phi \geq 0.80$, a broad L_3 peak spanning a wide Q range is observed at the low temperatures. The $\phi = 0.80$ spectra show that increasing the temperature above about 20 °C causes a transition between the L_3 phase and the droplet phase. However, microemulsions at the higher concentrations transform directly into the lamellar phase without the intervening droplet phase.

Further evidence for the lamellar L_α structure is the Fig. 4 plot of Q_1 against the surfactant volume fraction ϕ_s. The data are based on the first-order peak positions for both a range of volume fractions with W fixed at 40.8 and for a range of W's with $\phi = 0.80$. Assuming a repeat distance of $2\pi/Q_1$, an alternating arrangement of water and oil lamellar domains separated by AOT monolayers predicts that

$$Q_1 = \frac{\pi}{\delta}\phi_s , \tag{1}$$

where δ is the thickness of the surfactant layer. The slope of the fitted line in Fig. 4 yields a thickness of $\delta = 9.4 \pm 0.5$ Å, which is consistent with the value measured by neutron scattering for the length of the AOT tail [7].

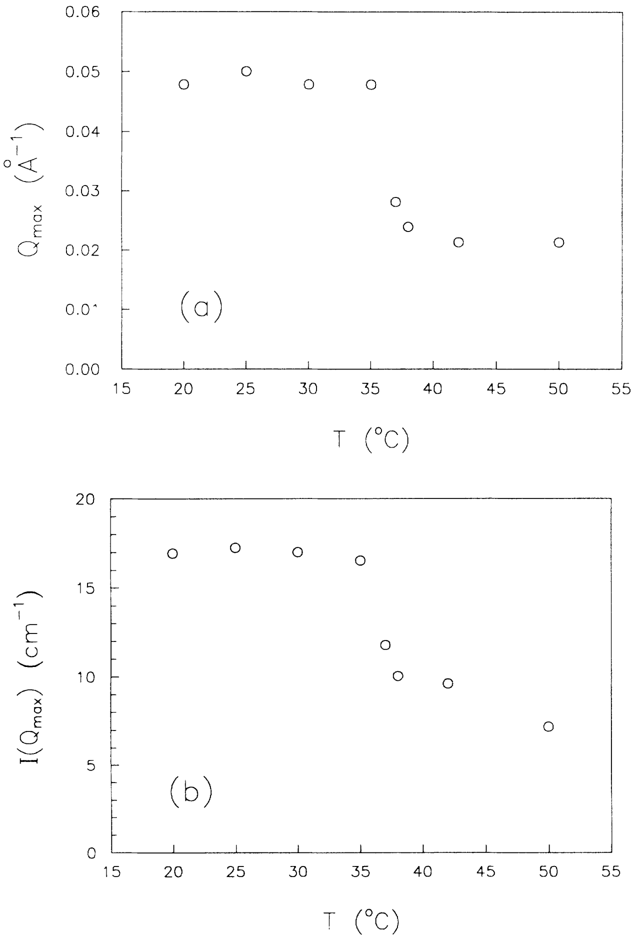

FIG. 3. Temperature dependence of (a) $Q_{\max}$, the scattering vector of the L_2 droplet peak, and (b) $I(Q_{\max})$, the corresponding peak intensity, from SAXS spectra at a volume fraction of $\phi = 0.76$.

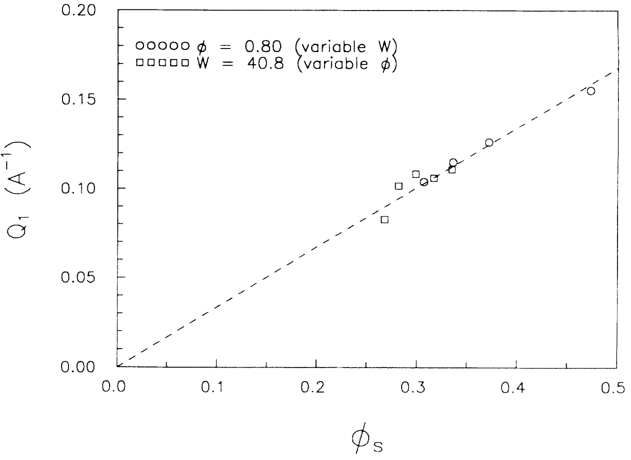

FIG. 4. Position of the first-order lamellar peak Q_1 as a function of surfactant volume fraction ϕ_s for spectra collected at a temperature of 50 °C.

It appears that information regarding the fluctuations of a surfactant layer in the lamellar phase can be extracted from the first- and second-order peak intensities, $I(Q_1)$ and $I(Q_2)$. At a given temperature, the SAXS spectrum can be represented as

$$I(Q,T) = e^{-Q^2\langle u^2(T)\rangle} I_{\text{rigid}}(Q) . \tag{2}$$

The exponential factor is the standard Debye-Waller factor [21,22], where $\langle u^2(T)\rangle$ is the mean-square fluctuation amplitude of the layer at temperature T. $I_{\text{rigid}}(Q)$ is the expected spectrum for a perfectly rigid lamellar structure. $\langle u^2(T)\rangle$ can be extracted by calculating the ratio of the measured L_α peak intensities. More specifically,

$$\langle u^2(T)\rangle = \ln\left[\frac{I(Q_1,T)}{I(Q_2,T)}\right] \Big/ 3Q_1^2 , \tag{3}$$

where we used the facts that $Q_2 = 2Q_1$ and $I_{\text{rigid}}(Q_1) = I_{\text{rigid}}(Q_2)$. Figure 5 is a graph of $\langle u^2\rangle$ vs T for the volume fraction $\phi = 0.76$. The data seem to indicate that $\langle u^2\rangle \propto T$, which is consistent with equipartition of energy [23]. At first glance the increase of $\langle u^2\rangle$ with T might seem marginal, however, the stated trend appears justified given the high precision of the peak positions and intensities used to obtain the Fig. 5 data points. According to a model for the thermal undulations of the lamellae [24], which predicts that the bilayers are flat on length scales smaller than a characteristic persistence length, the increased fluctuations we observe with increasing temperature may be a result of the predicted corresponding decrease in this persistence length. The root-mean-square fluctuation u_{rms} seems to be about the same as the thickness of the surfactant layer. This may reflect theoretical and experimental findings that systems having fluid-type lamellae are characterized by substantial repulsive layer-layer interactions due to out-of-plane layer fluctuations [25–27].

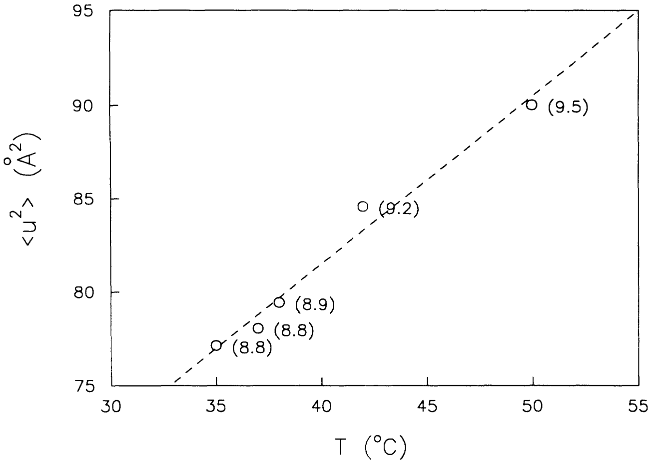

FIG. 5. Temperature dependence of the mean-square fluctuation amplitude $\langle u^2 \rangle$ for the lamellar phase at $\phi=0.76$. Each datum is labeled with the corresponding root-mean-square fluctuation amplitude u_{rms} in angstroms.

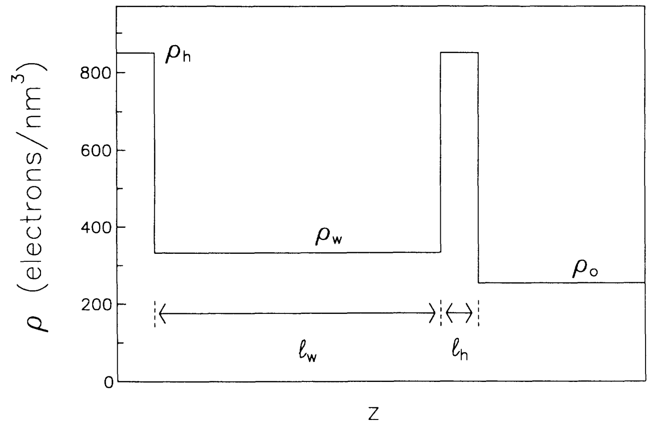

FIG. 6. Profile of electron density ρ along the axis of a lamellar stack. Only a single layer within the stack is shown. The electron densities of water, decane, and an AOT head group are denoted by ρ_w, ρ_0, and ρ_h, respectively. l_w and l_h represent the thicknesses of the water and head-group regions, respectively.

IV. PARACRYSTAL ANALYSIS OF THE L_α PHASE

A detailed structural analysis of the L_2 droplet phase based on small-angle neutron scattering (SANS) has previously been reported in the literature [4–6]. Our SAXS spectra for the L_2 phase are qualitatively similar to the SANS data, substantiating that the structure is that of densely packed water-in-oil droplets arranged in a disordered cubic lattice. In the present study, however, we choose to concentrate on obtaining detailed structural information on the lamellar phase. We realize that such a structure cannot be perfectly periodic in three dimensions, given samples of our size [28]. Therefore, we have assumed that the spectra can be reasonably interpreted using a variation on the one-dimensional paracrystal model [29]. The basic ansatz of the paracrystal theory is that the phase contains a Gaussian distribution of interlamellar spacings. With some rearrangement, the theory can be cast into the formalism based on an interparticle structure factor, in conjunction with an intraparticle form factor. The model appears to reliably fit the SAXS data for $Q \gtrsim 0.06$ Å^{-1}.

The assumption of our model is that the L_α phase contains a randomly oriented assembly of lamellar microdomains, or stacks, having a paracrystalline distortion. Each stack contains M correlated surfactant-water–surfactant-oil structural units, or bilayers, having a large lateral extent. The profile of the electron density (ρ) along the z axis, which defines the microdomain orientation, is depicted in Fig. 6. The electron densities of the water, decane oil, and AOT head group are, respectively, $\rho_w=333$ electrons/nm^3, $\rho_0=253$ electrons/nm^3, and $\rho_h=850$ electrons/nm^3 [30,31]. The AOT tails have essentially the same electron density as the oil and thus do not contribute to the scattering pattern in a significant way. The head-group diameter is given as $l_h=1.8$ Å [30,31], and the thickness of a water layer is

$$l_w=2\delta\phi_w/\phi_s=0.098W\delta \ . \tag{4}$$

δ, the thickness of the surfactant layer, is fixed at 9.4 Å, the value previously obtained from the analysis of Fig. 4. Thus the parameters of each layer within a lamellar stack are completely determined by W which, in turn, are fixed by the known microemulsion composition.

We assume that any scattering features due to interactions between different stacks do not appear in the Q range of our experiments (i.e., 0.01–0.25 Å^{-1}). As long as a typical stack consists of at least ten or so bilayers, prominent scattering features due to interplay between one stack and another would appear in the Q range below $\sim Q_1/10$. Since the first-order maxima in our SAXS spectra always appear in the neighborhood of ~ 0.1 Å^{-1}, we do not expect to observe such features. Rather, the scattering intensity from a sample containing a randomly oriented assembly of stacks is due to inter- and intralayer interference from within a stack. The scattering is thus given by the ensemble average [32]

$$I(Q)=\mathrm{const}\times\left\langle \sum_{j,k}^{M} f_j(Q,\mu) f_k^*(Q,\mu) e^{iQz_{jk}\mu} \right\rangle \ . \tag{5}$$

Here z_{jk} is the displacement between the jth and kth lamellae and μ is the cosine of the angle between the scattering vector $\mathbf{Q}$ and the z axis defined by the stack orientation. The const is a proportionality constant related to the number of stacks involved in scattering. $f(Q,\mu)$ is the form factor for a single layer within a stack of orientation μ and is computed by performing the following integration over the layer

$$f(Q,\mu)=\int_{\mathrm{layer}} [\rho(\mathbf{r})-\rho_0] e^{i\mathbf{Q}\cdot\mathbf{r}} d\mathbf{r} \ . \tag{6}$$

For random stack orientation, Eq. (5) can be reexpressed as the orientational average

$$I(Q)=\text{const}\times\int_0^1 P(Q,\mu)S(Q,\mu)d\mu \tag{7}$$

by defining the structure factor for a given stack orientation as

$$S(Q,\mu)=\frac{1}{M}\left\langle\sum_{j,k}^{M}e^{iQz_{jk}\mu}\right\rangle , \tag{8}$$

where $P(Q,\mu)=|f(Q,\mu)|^2$. The angular brackets in Eq. (8) represent an average over the distribution of interlamellar distances z_{jk}. Since the mean orientation of each bilayer is dictated by the orientation of the stack, one cannot decouple the form factor and structure factor when computing the orientational average of Eq. (7).

Following Ref. [33], we write the structure factor for a one-dimensional paracrystal based on assuming a Gaussian distribution of z_{jk}'s in Eq. (8):

$$S(Q,\mu)=Z(Q,\mu)+(1/M)I_c(Q,\mu) . \tag{9}$$

Here Z is the lattice factor given by

$$Z(Q,\mu)=\frac{(1-F^2)}{[1-2F\cos(Q\bar{d}\mu)+F^2]} , \tag{10}$$

where we define the following terms:

$$F(Q,\mu)=e^{-g^2\bar{d}^2Q^2\mu^2/2} , \tag{11}$$

$$I_c(Q,\mu)=\frac{-2F\{(1+F^2)\cos(Q\bar{d}\mu)-2F-F^M\cos[(M+1)Q\bar{d}\mu]+2F^{M+1}\cos(MQ\bar{d}\mu)-F^{M+2}\cos[(M-1)Q\bar{d}\mu]\}}{[1-2F\cos(Q\bar{d}\mu)+F^2]^2} . \tag{12}$$

In addition to M, the number of bilayers correlated in a stack, the structure factor depends on the parameters $\bar{d}$ and σ_d, which represent the mean and standard deviation of the interlamellar spacing, respectively. g is the so-called Hosemann g factor defined as $\sigma_d/\bar{d}$. In the limit $g\rightarrow 0$, Eq. (9) simply reduces to

$$S(Q,\mu)=(1/M)\frac{\sin^2(MQd\mu/2)}{\sin^2(Qd\mu/2)} , \tag{13}$$

which is the diffraction from M perfectly correlated lamellae of spacing d, with $z_{jk}=(j-k)d$.

In the case where the lateral dimension of a bilayer is much larger than the wavelength of the incident x rays, the orientational average of Eq. (7) can be handled in a much simpler, but exact, equivalent way [34] by replacing that expression with

$$I(Q)\simeq Q^{-2}P(Q,\mu=1)S(Q,\mu=1) . \tag{14}$$

The factor Q^{-2} is well known as the Lorentz factor. $Q^2I(Q)$ then represents the theoretical scattering pattern that would result along the direction defined by the axis of the stack if all stacks were perfectly aligned. The form factor for a layer in such a stack is calculated as

$$P(Q,\mu=1)=A^2\left[(\rho_w-\rho_0)l_w\frac{\sin(Ql_w/2)}{Ql_w/2}+2(\rho_h-\rho_0)l_h\frac{\sin(Ql_h/2)}{Ql_h/2}\times\cos[Q(l_w+l_h)/2]\right]^2 , \tag{15}$$

where A is the area of a layer. In our model, the form factor parameters are not adjustable.

The above paracrystal model with random stack orientation was used to fit the various SAXS spectra. The calculation of the scattered intensity from the model depends on the four fitting parameters $\bar{d}$, g, M, and a multiplicative normalization constant. Figure 7 shows representative fittings for spectra corresponding to $\phi=0.80$ at $T=50\,^\circ\mathrm{C}$, with various values of W. Data for $Q\lesssim 0.06$ Å^{-1} are not incorporated into the fit because the paracrystal model fails in the low-Q regime. However, the fit to the rest of the data appears reasonable at this concentration. The failure of the model at low Q may originate from neglecting aspects of the previously discussed repulsive interactions caused by layer fluctuations within a stack. One might expect the zero-order scattering to be suppressed more than the paracrystal model predicts due to decreased compressibility arising from entropic steric repulsion.

Table I lists the parameters obtained by fitting the paracrystal model to the $\phi=0.80$ L_α spectra as a function of W. The mean lamellar spacing $\bar{d}$ obtained from the fits is well represented by $2\pi/Q_1$. The Hosemann g factor, representing the variation of lamellar spacings, lies in the range 0.07–0.10. These values are consistent with standard paracrystal theory [29], which predicts that the

TABLE I. Dependence of the extracted paracrystal parameters on the molar ratio W. The volume fraction ϕ was 0.80 and the temperature was 50 °C.

W	$\bar{d}$ (Å)	g	M
15	39.9	0.081	14
25	48.2	0.075	14
30	53.8	0.081	14
35	58.5	0.079	15
40	60.7	0.097	15

second-order diffraction peak should be distinguishable from the background scattering if $g \lesssim 0.18$. M, the mean number of layers correlated in a stack, is about 14 or 15. In the paracrystal model, M is a parameter particularly sensitive to the low-Q data. However, because the fittings fail in this regime, the M values extracted were based on the high-Q data, and thus may not accurately reflect the true structure.

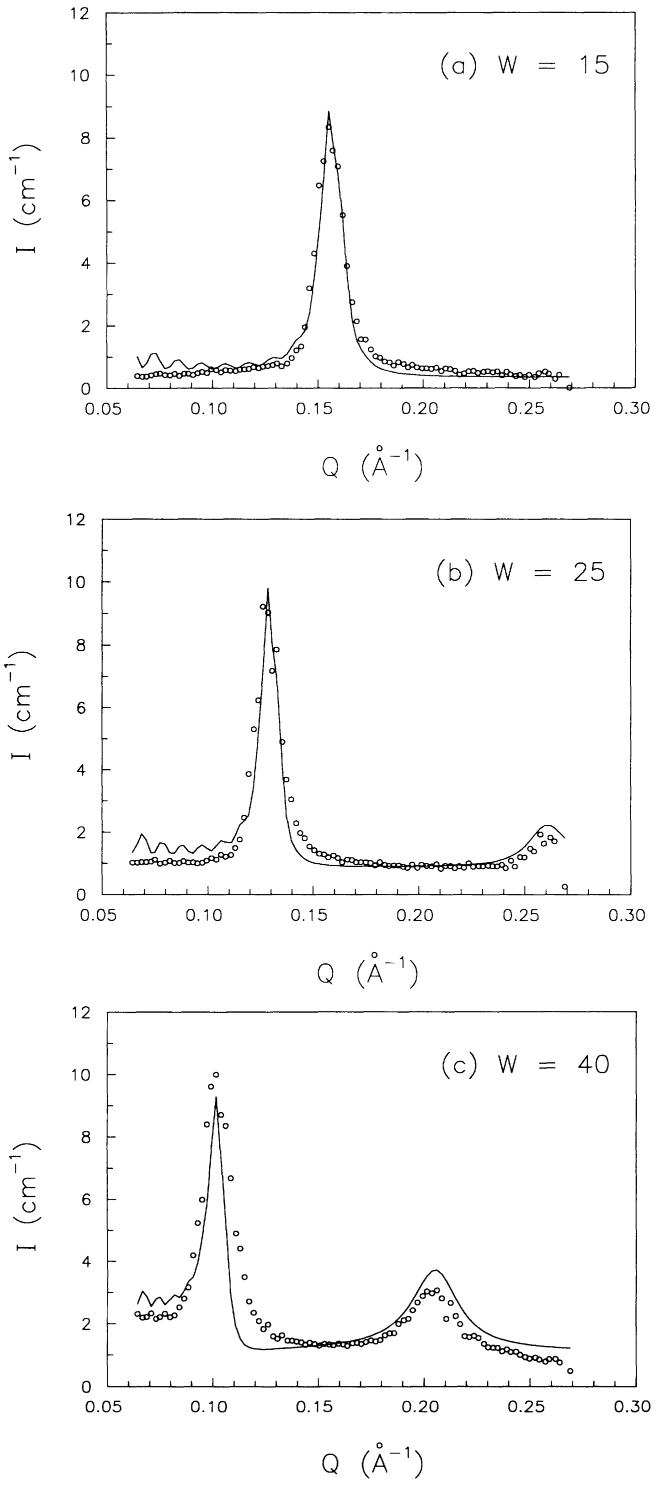

FIG. 7. SAXS spectra from the L_α phase at a volume fraction of $\phi=0.80$ and a temperature of 50 °C for three different water-to-AOT molar ratios. The solid curves are best fits to data using the paracrystal model.

V. TRANSPORT PROPERTIES AND DYNAMICS OF THE L_3 PHASE

Attempting a structural analysis of the L_3 phase poses a difficult problem since the characteristics of this phase are not yet well understood. In spite of the existence of freeze-fracture electron micrographs [35] for this type of phase that point to a structure resembling randomly connected lamellar sheets, the needed correlation function would be a difficult one to construct. Instead of attempting to model the detailed structure of the L_3 phase, we measured transport properties with the aim of characterizing dynamics resulting from the structure. Information was gained from dielectric-relaxation, shear-viscosity, and dynamic light-scattering experiments. We will look at the results of each type of measurement in turn.

Dielectric-relaxation measurements were performed at 1 MHz for $\phi=0.80$ and 0.85 microemulsions. Figure 8 shows the dielectric storage (ϵ') as a function of temperature. For $\phi=0.80$, a clear transition can be seen at about

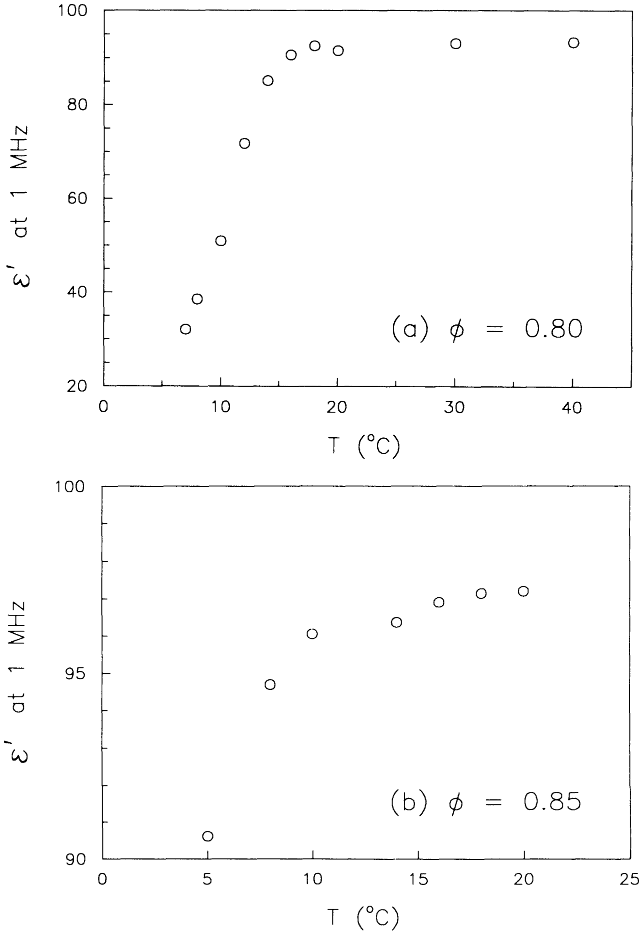

FIG. 8. Temperature dependence of the dielectric storage ϵ' at a frequency of 1 MHz for $\phi=0.80$ and 0.85.

20 °C, above which ϵ' levels off. This transition point is consistent with the SAXS data which show the existence of the L_3 phase at 20 °C and below. For $\phi=0.85$, a similar transition is observed at about 15 °C, which again is consistent with the SAXS measurements. These results suggest that the ϵ' measurement is a sensitive technique for measuring phase transitions in microemulsions. It also indicates that the lamellar phase has a higher dielectric tolerance than that of the L_3 phase, meaning that the correlation length corresponding to the lamellar structure is longer.

Figure 9(a) shows the viscosity (η) measured as a function of shear rate ($\dot{\gamma}$) for $\phi=0.75$ at various temperatures between 12 and 25 °C. For this entire temperature range, the system exhibits Newtonian behavior. This indicates that in the droplet phase, the system is a Newtonian fluid for shear rates up to 1500 s^{-1}. For $\phi=0.85$ [Fig. 9(b)], however, three striking features appear. First, for shear rates up to 790 s^{-1}, the system shows Newtonian behavior when in the L_3 phase ($T=3.7$, 10.5, and 15.7 °C), similar to the result reported for the cetylphridinium-chloride–hexanol–brine (0.2*M* NaCl) system [19]. Both results contradict the theoretical prediction of Cates *et al.* [15], which is based on passage shrinking and fusion processes. For shear rates above 790 s^{-1}, a drastic shear thinning is observed, indicating that the L_3 structure has ruptured. This also implies that the L_3 structural relaxation is on the order of 1 ms. Second, the zero-shear viscosity increased from 3.7 to 10.5 °C, but subsequently decreased toward the L_3-L_α phase boundary at 18.4 °C. This shows that the L_3 structure is temperature sensitive, and that the L_3 phase is a metastable one, thus functioning as a transition phase. Finally, the Newtonian properties start to decline for temperatures above 15.7 °C (approximately at the L_3-L_α phase boundary), exhibiting a strong shear thinning characteristic for $T=21.1$ °C, which is in the lamellar phase. In other words, the lamellar phase has a longer average correlation length than the L_3 phase, in agreement with our dielectric-relaxation results. Figure 10 shows the viscosity at $\phi=0.85$ as a function of temperature for a shear rate of 10 s^{-1}. A transition appears between 10 and 15 °C, again a result consistent with the SAXS and dielectric-relaxation data.

Quasielastic-light-scattering (QELS) measurements displayed two characteristic relaxation times for microemulsions in the L_3 phase, a fast and slow mode of about 1 ms and 1 s, respectively. These modes correspond to the relaxations of two structures of different length scales. Because the relaxation times are so different, the correlator sampling time was tuned to measure each relaxation mode separately. Figure 11 shows the intensity autocorrelation function versus the delay time for the $\phi=0.85$ microemulsion at $T=10$ °C. By applying a first cumulant analysis [36] to the slow component in Fig. 11(a), we obtain a relaxation time of about 1.5 s. We believe this corresponds to the Brownian motion of the entire interconnected sheet assembly of the L_3 structure. Analysis of the spectrum in Fig. 11(b) yields a relaxation time of about 780 μs. We believe this mode corresponds to the Brownian motion of a single lamellar sheet. Note that this relaxation time is similar to the one obtained from the shear-viscosity measurements.

Only one mode is observed for both the droplet and L_α phases, and the relaxation times are quite different from those in the L_3 phase. Figure 12 shows the relaxation

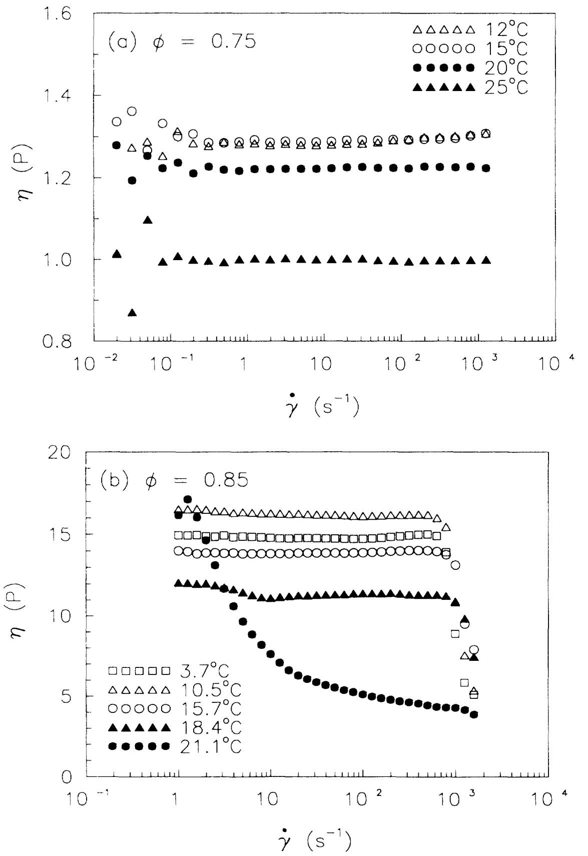

FIG. 9. Viscosity η as a function of shear rate $\dot{\gamma}$ at various temperatures for volume fractions (a) $\phi=0.75$ and (b) $\phi=0.85$.

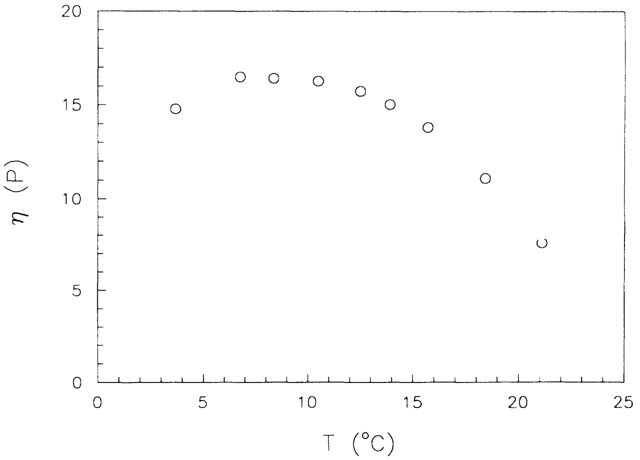

FIG. 10. Temperature dependence of the viscosity η at a shear rate of 10 s^{-1} for $\phi=0.85$.

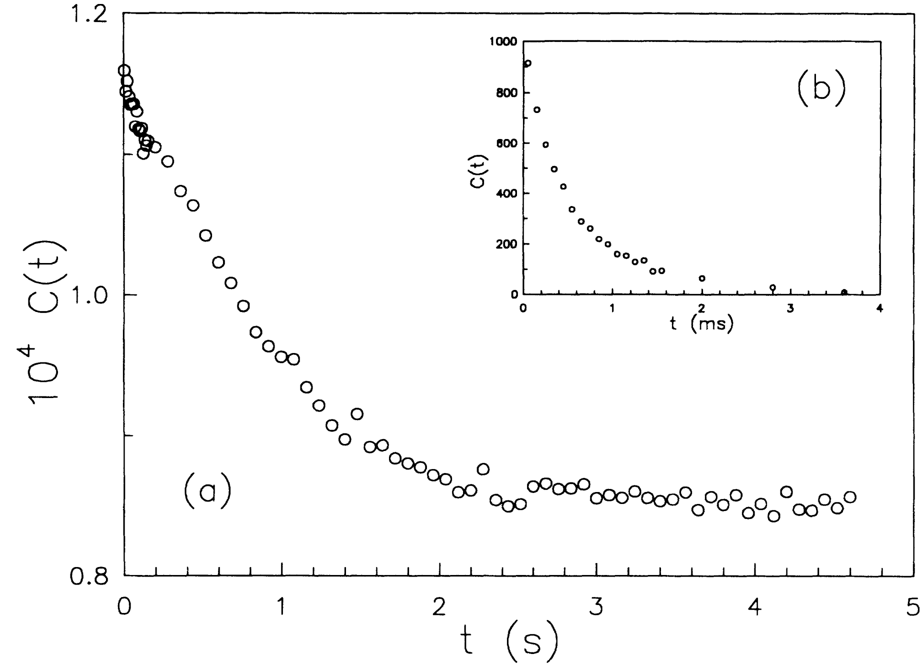

FIG. 11. Dynamic-light-scattering intensity autocorrelation function $C(t)$ vs delay time t for a sample of volume fraction $\phi=0.85$ at 10 °C. (a) The slow mode has a relaxation time of approximately 1.5 s. (b) The fast mode has a relaxation time of approximately 780 μs.

time as a function of volume fraction at $T=10$ °C. A marked discontinuity in the relaxation appears near $\phi\sim 0.8$, which is close to the L_2-L_3 phase boundary. In the figure, the data points above the transition correspond to the fast mode. One can see that the Brownian motion of a droplet is about two times slower than that of the single sheet in the L_3 structure. The L_α phase has a relaxation time on the order of several seconds.

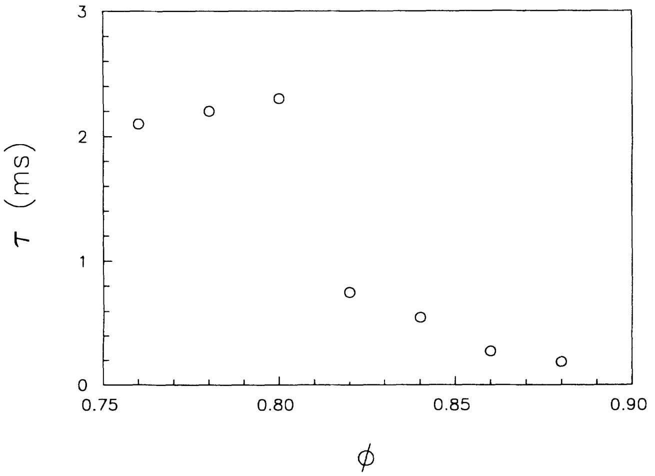

FIG. 12. Volume-fraction dependence of the relaxation time τ.

VI. CONCLUDING DISCUSSION

In this study, we have applied a variety of experimental techniques toward the mapping of a detailed phase diagram for the AOT-water-decane microemulsion system at high AOT-plus-water volume fractions ($0.60\le\phi\le 0.95$). We have found that the previously reported phase diagram [5] was not accurate for volume fractions in this range. The previous determination relied on simple techniques such as cloud-point observation, visualization through cross polarizers, as well as evaluation of optical and flow birefringence. Although these simple techniques may be quite adequate for some types of phase transitions, in the present study we found it necessary to implement a microprobe, namely x-ray scattering, to delineate the detailed structural transformations. Parts of the resulting phase diagram were then confirmed by supplementary measurements of the system's transport properties capable of providing information on dynamics.

The SAXS spectra clearly identify the droplet (L_2), lamellar (L_α), and randomly-connected lamellar (L_3) phases. In addition, a previously unrealized L_2-L_α coexistence region covering a wide range of temperatures has been identified. The L_2-to-L_α phase transition is found to be a first-order one. An L_3 phase was discovered in our system, forming at temperatures below the region of the L_α phase. It should be noted that an L_3 phase has also been reported as forming at temperatures below the L_α phase in the water-rich region of the pseudoternary AOT-brine-decane system [20]. Of course, unlike the dense L_3 phase investigated in our present study, formation of the latter phase requires the addition of a substantial amount of salt.

The structural characteristics of the lamellar L_α phase have been analyzed using a one-dimensional paracrystal model with random domain orientation. The lamellae are less than 100 Å apart, characterized by a spacing variation in the neighborhood of 8%. An analysis based solely on the positions and intensities of the first- and second-order scattering peaks indicate that the lamellae fluctuate with an amplitude comparable to the thickness of an intervening surfactant layer.

Information about the transitions near and properties of the L_3 phase were obtained from measurements of the dynamics. The dielectric-relaxation, shear-viscosity, and quasielastic light-scattering measurements were all found to be sensitive to the onset of structural transitions. This made them useful as companion tools for supporting parts of the phase diagram obtained from the SAXS data. Both the dielectric relaxation and the shear-viscosity measurements show that the correlation length of the L_3 structure is shorter than that of the lamellar structure. Our viscosity measurements are consistent with those of Snabre and Porte [19], showing the Newtonian behavior of the L_3 phase. However, the latter group did not quantitatively characterize the relaxation time of their system due to instrumentation limits on the shear rate. In our study, we varied the bob length to reach a shear rate of 1500 s^{-1} and found a relaxation time on the order of 1 ms, with no structural relaxation relevant in the range of about 10 ms to 10 s. These results are in contradiction to the non-Newtonian behavior expected in this range from the model proposed by Cates *et al.* [15]. The rheologically determined relaxation time is consistent with that obtained by analyzing the fast component of QELS spectra from the L_3 phase. We interpret this mode as corresponding to the Brownian motion of a single lamellar sheet, while the slow mode signals the motion of the entire interconnected sheet assembly.

ACKNOWLEDGMENTS

Acknowledgment is made to the Donors of the Petroleum Research Fund, administered by the American Chemical Society, for the partial support of this research (Grant No. 21202-GB7). The SAXS experiments performed at Oak Ridge National Laboratory were partially supported by the Division of Materials Sciences, U.S. Department of Energy under Contract No. DE-AC05-84OR21400 with Martin Marietta Energy Systems, Incorporated. SAXS experiments were also performed at the National Synchrotron Light Source, Station X12B, which is owned and operated by the Biology Department of the Brookhaven National Laboratory under funding from the Office of Health and Environmental Research, FWP KP04-01 and KP04-B043. We are grateful to J. S. Lin of ORNL for assistance with the 10-m small-angle scattering spectrometer. Special thanks are given to Rheometrics Inc. for granting us instrumentation time, and to R. Shar for providing indispensable assistance with the viscosity measurements. R. Strey provided helpful discussions regarding the microemuslion phase diagram. Sample preparation and tireless technical assistance were provided by M. M. De Tar.

---

[1] J. S. Huang, J. Surf. Sci. Technol. **5**, 83 (1989).

[2] S. H. Chen, T. L. Lin, and J. S. Huang, in *Physics of Complex and Supermolecular Fluids,* edited by S. A. Safran and N. A. Clark (Wiley, New York, 1987), p. 285.

[3] J. S. Huang, M. Kotlarchyk, and S. H. Chen, in *Micellar Solutions and Microemulsions: Structure, Dynamics, and Statistical Thermodynamics,* edited by S. H. Chen and R. Rajagopalan (Springer-Verlag, New York, 1990), p. 227.

[4] M. Kotlarchyk, S. H. Chen, J. S. Huang, and M. W. Kim, Phys. Rev. Lett. **53**, 941 (1984).

[5] E. Y. Sheu, S. H. Chen, J. S. Huang, and J. C. Sung, Phys. Rev. A **39**, 5867 (1989).

[6] M. Teubner and R. Strey, J. Chem. Phys. **87**, 3195 (1987).

[7] M. Kotlarchyk, S. H. Chen, J. S. Huang, and M. W. Kim, Phys. Rev. A **29**, 2054 (1984).

[8] S. H. Chen and J. S. Huang, Phys. Rev. Lett. **55**, 1888 (1985).

[9] S. H. Chen, J. Rouch, and P. Tartaglia, J. Non-Cryst. Solids **131-133**, 275 (1991).

[10] G. Porte, J. Marignan, P. Bassereau, and R. May, J. Phys. (Paris) **49**, 511 (1988).

[11] J. Marignan, J. Appell, P. Bassereau, G. Porte, and R. May, J. Phys. (Paris) **50**, 3553 (1989).

[12] D. Gazeau, A. M. Bellocq, D. Roux, and T. Zemb, Europhys. Lett. **9**, 447 (1989).

[13] R. Strey, R. Schomacker, D. Roux, F. Nallet, and U. Olsson, J. Chem. Soc. Faraday Trans. **86**, 2253 (1990).

[14] G. Porte, J. Appell, P. Bassereau, and J. Marignan, J. Phys. (Paris) **50**, 1335 (1989).

[15] M. E. Cates, D. Roux, D. Andelman, S. T. Milner, and S. A. Safran, Europhys. Lett. **5**, 733 (1988).

[16] M. E. Cates and S. T. Milner, Phys. Rev. Lett. **62**, 1856 (1989).

[17] M. E. Cates and D. Roux, J. Phys.: Condens. Matter **2**, SA339 (1990).

[18] M. E. Cates, Physica A **176**, 187 (1991).

[19] P. Snabre and G. Porte, Europhys. Lett. **13**, 641 (1990).

[20] S. H. Chen, S. L. Chang, R. Strey, and P. Thiyagarajan, J. Phys.: Condens. Matter **3**, F91 (1991).

[21] B. T. M. Willis and A. W. Pryor, *Thermal Vibrations in Crystallography* (Cambridge University Press, Cambridge, England, 1975).

[22] A. J. C. Wilson, *Elements of X-Ray Crystallography* (Addison-Wesley, Reading, MA, 1970).

[23] D. A. McQuarrie, *Statistical Mechanics* (Harper & Row, New York, 1976).

[24] P. G. De Gennes and C. Taupin, J. Phys. Chem. **86**, 2294 (1982).

[25] W. Helfrich, Z. Naturforsch. Teil A **33**, 305 (1978).

[26] C. R. Safinya, D. Roux, G. S. Smith, S. K. Sinha, P. Di-

mon, N. A. Clark, and A. M. Bellocq, Phys. Rev. Lett. **57**, 2718 (1986).

[27] C. R. Safinya, E. B. Sirota, D. Roux, and G. S. Smith, Phys. Rev. Lett. **62**, 1134 (1989).

[28] R. E. Peierls, Helv. Phys. Acta, Suppl. **7**, 81 (1934).

[29] R. Hosemann and S. N. Bagchi, *Direct Analysis of Diffraction by Matter* (North-Holland, Amsterdam, 1962).

[30] C. Robertus, J. G. H. Joosten, and Y. K. Levine, Prog. Colloid Polym. Sci. **77**, 115 (1988).

[31] L. Auvray, J. P. Cotton, R. Ober, and C. Taupin, J. Phys. (Paris) **45**, 913 (1984).

[32] M. Kotlarchyk and S. H. Chen, J. Chem. Phys. **79**, 2461 (1983).

[33] T. Hashimoto, A. Todo, and H. Kawai, Polym. J. **10**, 521 (1978).

[34] M. Shibayama and T. Hashimoto, Macromolecules **19**, 740 (1986).

[35] R. Strey, W. Jahn, G. Porte, and P. Bassereau, Langmuir **6**, 1635 (1990).

[36] D. E. Koppel, J. Chem. Phys. **57**, 4814 (1972).